Chinese Journal of Aeronautics, (2016), 29(4): 1052–1064

Chinese Society of Aeronautics and Astronautics
& Beihang University

Chinese Journal of Aeronautics

cja@buaa.edu.cn
www.sciencedirect.com

Optimal terminal guidance for exoatmospheric interception

Yu Wenbin, Chen Wanchun, Yang Liang *, Liu Xiaoming, Zhou Hao

School of Astronautics, Beihang University, Beijing 100083, China

Received 1 October 2015; revised 7 December 2015; accepted 7 March 2016
Available online 23 June 2016

KEYWORDS

Exoatmospheric interception;
Explicit guidance;
Guidance;
Optimal control;
Proportional navigation;
Pulsed guidance

Abstract In this study, two optimal terminal guidance (OTG) laws, one of which takes into account the final velocity vector constraint, are developed for exoatmospheric interception using optimal control theory. In exoatmospheric interception, because the proposed guidance laws give full consideration to the effect of gravity, they consume much less fuel than the traditional guidance laws while requiring a light computational load. In the development of the guidance laws, a unified optimal guidance problem is put forward, where the final velocity vector constraint can be considered or neglected by properly adjusting a parameter in the cost function. To make this problem analytically solvable, a linear model is used to approximate the gravity difference, the difference of the gravitational accelerations of the target and interceptor. Additionally, an example is provided to show that some achievements of this study can be used to significantly improve the fuel efficiency of the pulsed guidance employed by the interceptor whose divert thrust level is fixed.

1. Introduction

As the maximum speed of intercontinental ballistic missile (ICBM) is greater than 7 km/s and sometimes its apogee altitude can be up to 2000 km, currently only the ground-based midcourse defense (GMD) system equipped with ground-based interceptor (GBI) missile has the capability of intercepting ICBM. The flight of GBI generally has three phases: boost, coast, and terminal guidance phases. After launch, the booster tries to put its warhead, which is commonly called kinetic kill vehicle (KKV) and destroys its intended target by direct collision, on a collision course, which means that if the KKV and target are only governed by gravity, the KKV can just hit the target directly. After the booster is turned off, the KKV is separated from the booster and enters the coast phase in which the KKV flies to the predicted intercept point (PIP) without control. When the distance between the KKV and target reduces to a specified value, the terminal guidance phase begins. At this phase, the KKV uses the divert thrusters to perform lateral maneuvers in order to eliminate the PIP error. When these thrusters work, they consume much fuel. Therefore, one main concern of designing the terminal guidance law is to minimize the maneuvering energy so as to save fuel. Additionally, sometimes it is desired that the KKV collides head-on with the target to increase the chances of success. Therefore, the paper is

* Corresponding author. Tel.: +86 10 82339226.
E-mail address: yangliang.buaa@hotmail.com (L. Yang).
Peer review under responsibility of Editorial Committee of CJA.

Production and hosting by Elsevier

http://dx.doi.org/10.1016/j.cja.2016.04.019
1000-9361

aimed at designing two fuel-saving terminal guidance laws for exoatmospheric interception, one of which further considers the final velocity vector constraint.

The most widely used guidance law is proportional navigation (PN) because of its simplicity, effectiveness, and ease of implementation.[1] Yuan first put forward the basic principle of PN:[2] if the interceptor turns at a rate proportional to that of the line of sight (LOS), the interceptor can successfully hit the target travelling in uniform linear motion, and the angular velocity of the LOS will become zero finally. Adler extended PN to a 3D one using the tool of solid geometry.[3] Bryson and Ho demonstrated the optimality of PN.[4] Zarchan evaluated the performance of PN thoroughly and deeply.[1] In Refs.[5–11], the variants of PN and their closed form solutions were presented. Graber developed the so-called augmented proportional navigation (APN) by adding an extra term to PN to account for the constant maneuvering acceleration of target.[12] In Ref.[13], the guidance law considering the response lags was presented. Turetsky and Shinar proposed the guidance laws based on pursuit-evasion game formulations.[14] Ge et al. developed a head-pursuit guidance law for 3D hypervelocity interception using Lyapunov stability theory.[15]

For some special missions, the guidance laws capable of shaping trajectory are needed. These guidance laws are collectively referred to as trajectory shaping guidance (TSG). Cherry proposed a simple and effective TSG, called explicit guidance (E Guidance), for the first time by assuming that the commanded acceleration is a polynomial function of time.[16] E Guidance can be treated as an extension of PN because its expression consists of two terms: one is PN used to steer missile to destination, the other is used to control the final velocity vector. Ohlmeyer and Phillips obtained a series of the E Guidance coefficients by solving an optimal control problem with time-to-go weighted cost function.[17] Yu and Chen obtained the generalized closed form solutions of E Guidance where the closing speed can be an arbitrary positive function of time.[18] Further, by analyzing these generalized solutions, the stability domain of the guidance coefficients was obtained, in which E Guidance is stable and the commanded accelerations tend to be zero finally. Wang et al. improved E Guidance by considering the constant maneuvering acceleration of target.[19] In Refs.[20–24], other types of TSG were presented. Yu and Chen proposed a novel guidance law for guiding missile against a maneuvering target while satisfying a circular no-fly-zone constraint.[7] In this guidance law, the real space is distorted such that the boundary of the no fly zone becomes a straight line, and then PN is used to steer the missile to the virtual target in the distorted space.

The widely-used terminal guidance laws for exoatmospheric interception are PN, APN, and predictive guidance (PG). Here, PG[1] is a guidance law that conducts the trajectory simulation once in each guidance cycle to predict the zero-effort miss (ZEM), and then uses the predicted ZEM to generate acceleration command. Zarchan evaluated their performance.[1] Simulation results show that PG consumes the least fuel because PG uses the accurate gravity model, but requires the heaviest computational load due to the real-time onboard trajectory simulations. PN and APN cause the interceptor to perform unnecessary maneuvers even if the interceptor has already been on a collision course. This is because they use the inaccurate gravity models: PN implies that the gravity difference is zero, whereas APN assumes that the gravity difference is constant. Simulation results show that the amount of the wasted fuel of APN is about half that of PN.

In this paper, two optimal terminal guidance (OTG) laws are developed for exoatmospheric interception using the optimal control theory: one considers the final velocity vector constraint, whereas the other does not consider it. Because the developed guidance laws evaluate the effect of gravity more accurately and need not conduct any onboard trajectory simulation, they almost consume as little fuel as PG while having a light computational load. In the development of the OTG laws, a unified optimal guidance problem is put forward, of which the developed guidance laws are the two special solutions. Because the real gravity is a complex nonlinear function of position, it is impossible to obtain the exact analytical solutions of the problem. However, by observing the simulation trials, it can be found that the gravity difference almost varies linearly with time. Therefore, the problem is made analytically solvable by the innovative use of a linear gravity difference model. Additionally, as the angular velocity of LOS can be measured by seeker directly, the OTG laws are reformulated in terms of the angular velocity of LOS using a novel 3D transformation method based on vector operations, which considers the effect of gravity difference.

To implement the OTG laws, the position information is needed. However, the onboard infrared seeker can only provide the LOS orientation information and has a limited detection distance. Thus, in practice, the information on the states of motion is mainly provided by the external detection system such as X-band radar. When the interceptor gets close enough to the target, the infrared seeker becomes activated, and the data detected by the infrared seeker and external detection system are fused by Kalman filter to improve the accuracy of data.

It should be mentioned that some kinds of KKV cannot be throttled. For these KKVs, every time the thruster is turned on, the thrust will reach a fixed level and cannot be adjusted. In such a case, the pulsed guidance laws[1,25,26] are commonly employed, which use the predicted ZEM to determine the duration time of thrust. However, these guidance laws neglect the effect of gravity when predicting the ZEM. Therefore, they will also result in a great waste of fuel in the long-range exoatmospheric interception. In fact, the formula of predicting ZEM proposed in this paper can be applied to the pulsed guidance laws. In Section 6.3, an example is given to demonstrate that this can significantly improve the fuel efficiency of the pulsed guidance laws.

2. Equations of motion

Fig. 1 depicts the 3D engagement geometry outside the atmosphere of Earth. In this figure, the center of Earth is assumed to be stationary in the inertial space. An inertial frame of reference with origin at the center of Earth is created and called frame F_E. As the engagement is outside the atmosphere, the interceptor missile uses the divert thrusters to perform lateral maneuvers where the thrust acceleration vector is denoted as $\boldsymbol{a}_M = [a_{Mx}, a_{My}, a_{Mz}]^T$. The target is only governed by gravity and thus flies ballistically. In frame F_E, the position vectors of the interceptor missile and target are denoted as $\boldsymbol{X}_M = [x_M, y_M, z_M]^T$ and $\boldsymbol{X}_T = [x_T, y_T, z_T]^T$ respectively, their velocity vectors are denoted as $\boldsymbol{V}_M = [V_{Mx}, V_{My}, V_{Mz}]^T$ and

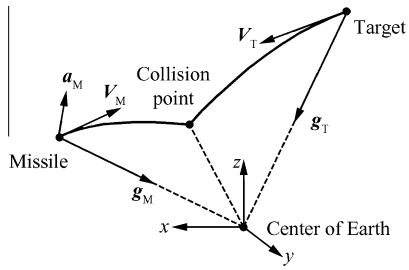

Fig. 1 Exoatmospheric interception geometry.

$\boldsymbol{V}_T = [V_{Tx}, V_{Ty}, V_{Tz}]^T$ respectively, and their gravitational acceleration vectors are denoted as $\boldsymbol{g}_M$ and $\boldsymbol{g}_T$ respectively.

The equations of motion are

$$\dot{\boldsymbol{X}}_M = \boldsymbol{V}_M \tag{1}$$

$$\dot{\boldsymbol{V}}_M = \boldsymbol{a}_M + \boldsymbol{g}_M \tag{2}$$

$$\dot{\boldsymbol{X}}_T = \boldsymbol{V}_T \tag{3}$$

$$\dot{\boldsymbol{V}}_T = \boldsymbol{g}_T \tag{4}$$

where $\boldsymbol{g}_M$ and $\boldsymbol{g}_T$ are determined by

$$\boldsymbol{g}_M = -\frac{\mu \boldsymbol{X}_M}{||\boldsymbol{X}_M||^3}, \boldsymbol{g}_T = -\frac{\mu \boldsymbol{X}_T}{||\boldsymbol{X}_T||^3} \tag{5}$$

where μ is a constant of about 3.96272×10^{14} m^3/s^2, and the symbol "$||\cdot||$" means the Euclidean norm of vector.

3. Optimal guidance problem

To develop the fuel-efficient guidance laws for exoatmospheric interception, the optimal guidance problem is posed where the cost function is

$$J = \frac{1}{2}k\left(\boldsymbol{V}_{TMf} - \boldsymbol{V}^*_{TMf}\right)^T\left(\boldsymbol{V}_{TMf} - \boldsymbol{V}^*_{TMf}\right) + \int_0^{t_f} \frac{\boldsymbol{a}_M^T \boldsymbol{a}_M}{2t_{go}^n} \mathrm{d}t \tag{6}$$

subject to the dynamic constraints

$$\dot{\boldsymbol{X}}_{TM} = \boldsymbol{V}_{TM} \tag{7}$$

$$\dot{\boldsymbol{V}}_{TM} = -\boldsymbol{a}_M + \boldsymbol{g}_{TM} \tag{8}$$

and the final condition

$$\boldsymbol{X}_{TMf} = \boldsymbol{0} \tag{9}$$

Here, k is a constant. t_f represents the end time or flight time and will be discussed in detail in Section 5. $t_{go} = t_f - t$ is the time to go. $\boldsymbol{X}_{TM} = \boldsymbol{X}_T - \boldsymbol{X}_M$ and $\boldsymbol{V}_{TM} = \boldsymbol{V}_T - \boldsymbol{V}_M$ are the position and velocity vectors of the target relative to the missile, respectively. $\boldsymbol{X}_{TMf}$ is the final value of $\boldsymbol{X}_{TM}$, and Eq. (9) makes the missile collide with the target. $\boldsymbol{V}_{TMf}$ is the final value of $\boldsymbol{V}_{TM}$. $\boldsymbol{V}^*_{TMf}$ is the desired value of $\boldsymbol{V}_{TMf}$. $\boldsymbol{g}_{TM} = \boldsymbol{g}_T - \boldsymbol{g}_M$ is the gravity difference.

The cost function is designed with specific purposes. The first term on the right side of Eq. (6) is proposed for achieving the desired final velocity vector. In this term, the parameter k is used to adjust the contribution of $\boldsymbol{V}_{TMf}$ to the cost function. After obtaining the general analytical solution of the optimal guidance problem, if one lets $k = 0$, the guidance law without constraint on $\boldsymbol{V}_{TMf}$ can be obtained, but if one lets k go to infinity, the guidance law will be obtained, which makes the missile collide with its target while satisfying $\boldsymbol{V}_{TMf} = \boldsymbol{V}^*_{TMf}$. The second term on the right side of Eq. (6) comes from Ref.[17] and is used to minimize the lateral divert requirement so as to save fuel. In this term, as t goes to t_f, the weight $(1/t_{go}^n)$ tends to infinity. This makes $\boldsymbol{a}_M$ converge to zero finally, and greater exponent n tends to accelerate the convergence speed. It is emphasized again that different from the previous studies[4,12,17,19], the effect of the gravity difference, which varies with position, is considered here. Thus, the proposed guidance laws require much less fuel than the traditional ones in exoatmospheric interception.

4. Optimal terminal guidance laws

As $\boldsymbol{g}_{TM}$ is a complex nonlinear vector function of position, the analytical solution of the posed optimal guidance problem cannot be obtained. However, by observing the simulation trials where both the missile and target are only governed by gravity, it can be found that if the missile is just on a collision course, $\boldsymbol{g}_{TM}$ varies almost linearly with time, and at the collision point, there is $\boldsymbol{g}_{TM} = \boldsymbol{0}$. As an example, one of these simulation trials is presented in Figs. 2 and 3. Here, Fig. 2 shows the trajectories of the missile and target, and Fig. 3 shows the histories of $\boldsymbol{g}_{TM}$.

Further, it is concerned about whether the missile's maneuver will seriously worsen the degree of linearity of $\boldsymbol{g}_{TM}$. Therefore, it is needed to analyze the influence of the trajectory adjustment on $\boldsymbol{g}_{TM}$ quantificationally. Define $\boldsymbol{X}^*_M$ and $\boldsymbol{X}^*_T$ as the nominal trajectories of the missile and target respectively where the missile flies without control and can just hit the target. Define $\boldsymbol{g}^*_{TM}$ as the gravity difference corresponding to the nominal trajectories. Define $\Delta\boldsymbol{X}_M$ as the difference of the actual and nominal trajectories of the missile. Thus, the actual missile trajectory is $\boldsymbol{X}_M = \boldsymbol{X}^*_M + \Delta\boldsymbol{X}_M$. Then, there is

$$\boldsymbol{g}_{TM} = \frac{\mu(\boldsymbol{X}^*_M + \Delta\boldsymbol{X}_M)}{||\boldsymbol{X}^*_M + \Delta\boldsymbol{X}_M||^3} - \frac{\mu\boldsymbol{X}^*_T}{||\boldsymbol{X}^*_T||^3} \tag{10}$$

The first order Taylor approximation of Eq. (10) is

$$\begin{aligned}\boldsymbol{g}_{TM} \approx\ & \frac{\mu\boldsymbol{X}^*_M}{||\boldsymbol{X}^*_M||^3} + \frac{\mu\Delta\boldsymbol{X}_M}{||\boldsymbol{X}^*_M||^3} \\ & - \frac{3\mu\boldsymbol{X}^*_M}{||\boldsymbol{X}^*_M||^4}\frac{\left(\boldsymbol{X}^*_M\right)^T\Delta\boldsymbol{X}_M}{\sqrt{\left(\boldsymbol{X}^*_M\right)^T\boldsymbol{X}^*_M}} - \frac{\mu\boldsymbol{X}^*_T}{||\boldsymbol{X}^*_T||^3} \\ & = \boldsymbol{g}^*_{TM} + \frac{\mu}{||\boldsymbol{X}^*_M||^2}\left(\boldsymbol{I} - \frac{3\boldsymbol{X}^*_M\left(\boldsymbol{X}^*_M\right)^T}{||\boldsymbol{X}^*_M||^2}\right)\frac{\Delta\boldsymbol{X}_M}{||\boldsymbol{X}^*_M||}\end{aligned} \tag{11}$$

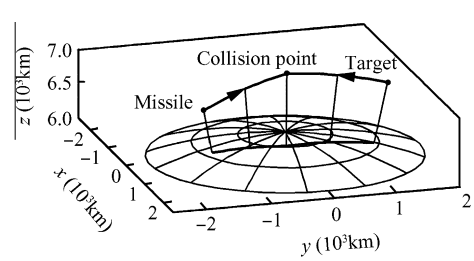

Fig. 2 Nominal trajectories of missile and target.

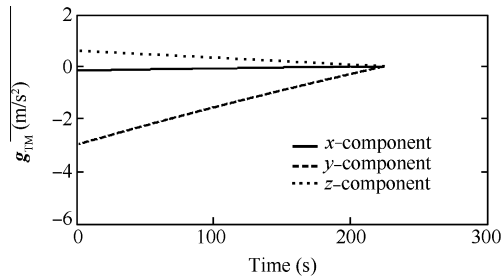

Fig. 3 $\boldsymbol{g}_{\mathrm{TM}}$ almost changes linearly with time in nominal case.

In fact, the PIP error due to the boost guidance will not exceed 50 km. So the terminal guidance only needs to adjust the trajectory slightly but accurately, and $||\Delta \boldsymbol{X}_{\mathrm{M}}||$ is generally less than 50 km. By contrast, $||\boldsymbol{X}^*_{\mathrm{M}}||$ is greater than the Earth's radius of about 6356 km. Therefore, $||\Delta \boldsymbol{X}_{\mathrm{M}}||/||\boldsymbol{X}^*_{\mathrm{M}}|| < 0.01$. Meanwhile, $\mu/||\boldsymbol{X}^*_{\mathrm{M}}||^2$ has the same order of magnitude as $\boldsymbol{g}^*_{\mathrm{TM}}$. Thus, the change in $\boldsymbol{g}_{\mathrm{TM}}$ due to the trajectory adjustment is almost two orders of magnitude smaller than $\boldsymbol{g}^*_{\mathrm{TM}}$. Thereby, it can be concluded that $\boldsymbol{g}_{\mathrm{TM}}$ still varies almost linearly with time even if the missile trajectory is adjusted by the divert thrusts. Thus, it is reasonable to use the following linear model[27] to approximate the gravity difference

$$\boldsymbol{g}_{\mathrm{TM}} = \boldsymbol{g}_{\mathrm{TM0}} \frac{t_{\mathrm{f}} - t}{t_{\mathrm{f}}} \tag{12}$$

where $\boldsymbol{g}_{\mathrm{TM0}}$ is the initial value of $\boldsymbol{g}_{\mathrm{TM}}$. This linear model was first proposed by Newman and used to develop an iterative guidance law for steering booster.[27] However, compared with traditional guidance laws such as Lambert guidance, the developed guidance has a poor performance. For instance, if the initial distance is about 4000 km, the miss distance can be up to 5 km. Therefore, Newman further used two more complicated but more accurate models to improve the guidance law. Different from the boost case, the linear model is very suitable for designing the terminal guidance, because (1) the linear model will not result in missing the target since the trajectory correction is always conducted until the collision occurs; (2) the linear model makes the optimal guidance problem analytically solvable, even though the problem-solving process is complicated and full of mathematic tricks; (3) the developed terminal guidance laws are expressed as explicit functions of current states, which are elegant in form and easy to implement; (4) compared with traditional terminal guidance laws, the new guidance laws can significantly reduce the fuel consumption.

According to optimal control theory[4], using the linear model, the Hamiltonian is

$$\begin{aligned} H &= \frac{\boldsymbol{a}_{\mathrm{M}}^{\mathrm{T}} \boldsymbol{a}_{\mathrm{M}}}{2(t_{\mathrm{f}} - t)^n} + \boldsymbol{\lambda}_1^{\mathrm{T}} \boldsymbol{V}_{\mathrm{TM}} \\ &\quad + \boldsymbol{\lambda}_2^{\mathrm{T}} \left(-\boldsymbol{a}_{\mathrm{M}} + \frac{\boldsymbol{g}_{\mathrm{TM0}}}{t_{\mathrm{f}}} (t_{\mathrm{f}} - t) \right) \end{aligned} \tag{13}$$

where $\boldsymbol{\lambda}_1$ and $\boldsymbol{\lambda}_2$ are Lagrange multiplier vector functions. To facilitate writing, a new notation for partial derivative is defined as follows.

If there is a multivariable function $z = f(\boldsymbol{X}, \boldsymbol{Y})$ where $\boldsymbol{X} = [x_1, x_2, \cdots, x_n]^{\mathrm{T}}$ and $\boldsymbol{Y} = [y_1, y_2, \cdots, y_m]^{\mathrm{T}}$, then define the partial derivatives of z with respect to $\boldsymbol{X}$ and $\boldsymbol{Y}$ as

$$\begin{cases} \dfrac{\partial z}{\partial \boldsymbol{X}} = \left[\dfrac{\partial z}{\partial x_1}, \dfrac{\partial z}{\partial x_2}, \cdots, \dfrac{\partial z}{\partial x_n} \right]^{\mathrm{T}} \\ \dfrac{\partial z}{\partial \boldsymbol{Y}} = \left[\dfrac{\partial z}{\partial y_1}, \dfrac{\partial z}{\partial y_2}, \cdots, \dfrac{\partial z}{\partial y_m} \right]^{\mathrm{T}} \end{cases} \tag{14}$$

Consequently, the co-state equations are

$$\dot{\boldsymbol{\lambda}}_1 = -\frac{\partial H}{\partial \boldsymbol{X}_{\mathrm{TM}}} = \boldsymbol{0} \tag{15}$$

$$\dot{\boldsymbol{\lambda}}_2 = -\frac{\partial H}{\partial \boldsymbol{V}_{\mathrm{TM}}} = -\boldsymbol{\lambda}_1 \tag{16}$$

The stationarity condition is

$$\frac{\partial H}{\partial \boldsymbol{a}_{\mathrm{M}}} = \frac{1}{(t_{\mathrm{f}} - t)^n} \boldsymbol{a}_{\mathrm{M}} - \boldsymbol{\lambda}_2 = \boldsymbol{0} \tag{17}$$

Denote the first term on the right side of the cost function (Eq. (6)) as

$$\phi = \frac{1}{2} k (\boldsymbol{V}_{\mathrm{TMf}} - \boldsymbol{V}^*_{\mathrm{TMf}})^T (\boldsymbol{V}_{\mathrm{TMf}} - \boldsymbol{V}^*_{\mathrm{TMf}}) \tag{18}$$

As $\boldsymbol{V}_{\mathrm{TMf}}$ is not specified in the posed optimal guidance problem, the final value of $\boldsymbol{\lambda}_2$ should satisfy the following condition to minimize the cost function

$$\boldsymbol{\lambda}_{2\mathrm{f}} = \frac{\partial \phi}{\partial \boldsymbol{V}_{\mathrm{TMf}}} = k\left(\boldsymbol{V}_{\mathrm{TMf}} - \boldsymbol{V}^*_{\mathrm{TMf}}\right) \tag{19}$$

Integrating Eqs. (15) and (16) and then using Eq. (19), we obtain

$$\boldsymbol{\lambda}_1 = \boldsymbol{C}_1 \tag{20}$$

$$\boldsymbol{\lambda}_2 = \boldsymbol{C}_1 (t_{\mathrm{f}} - t) + k\left(\boldsymbol{V}_{\mathrm{TMf}} - \boldsymbol{V}^*_{\mathrm{TMf}}\right) \tag{21}$$

where $\boldsymbol{C}_1$ is a undetermined constant vector. Substituting Eq. (21) into Eq. (17) yields

$$\boldsymbol{a}_{\mathrm{M}} = \boldsymbol{C}_1 (t_{\mathrm{f}} - t)^{n+1} + k(\boldsymbol{V}_{\mathrm{TMf}} - \boldsymbol{V}^*_{\mathrm{TMf}})(t_{\mathrm{f}} - t)^n \tag{22}$$

Substituting Eqs. (12) and (22) into Eq. (8) and then integrating Eq. (8), we obtain

$$\begin{aligned} \boldsymbol{V}_{\mathrm{TM}} &= \boldsymbol{V}_{\mathrm{TM0}} + \frac{1}{2} \boldsymbol{g}_{\mathrm{TM0}} t_{\mathrm{f}} - \frac{1}{n+2} \boldsymbol{C}_1 t_{\mathrm{f}}^{n+2} \\ &- \frac{k\left(\boldsymbol{V}_{\mathrm{TMf}} - \boldsymbol{V}^*_{\mathrm{TMf}}\right) t_{\mathrm{f}}^{n+1}}{n+1} - \frac{\boldsymbol{g}_{\mathrm{TM0}}}{2 t_{\mathrm{f}}} (t_{\mathrm{f}} - t)^2 \\ &+ \frac{\boldsymbol{C}_1 (t_{\mathrm{f}} - t)^{n+2}}{n+2} + \frac{k\left(\boldsymbol{V}_{\mathrm{TMf}} - \boldsymbol{V}^*_{\mathrm{TMf}}\right)(t_{\mathrm{f}} - t)^{n+1}}{n+1} \end{aligned} \tag{23}$$

Substituting Eq. (23) into Eq. (7) and then integrating Eq. (7), we obtain

$$\begin{aligned} \boldsymbol{X}_{\mathrm{TM}} &= \boldsymbol{X}_{\mathrm{TM0}} + \boldsymbol{V}_{\mathrm{TM0}} t + \frac{1}{2} \boldsymbol{g}_{\mathrm{TM0}} t_{\mathrm{f}} t - \frac{1}{6} \boldsymbol{g}_{\mathrm{TM0}} t_{\mathrm{f}}^2 \\ &- \frac{1}{n+2} \boldsymbol{C}_1 t_{\mathrm{f}}^{n+2} t - \frac{1}{n+1} k(\boldsymbol{V}_{\mathrm{TMf}} - \boldsymbol{V}^*_{\mathrm{TMf}}) t_{\mathrm{f}}^{n+1} t \\ &+ \frac{\boldsymbol{g}_{\mathrm{TM0}}}{6 t_{\mathrm{f}}} (t_{\mathrm{f}} - t)^3 - \frac{\boldsymbol{C}_1 (t_{\mathrm{f}} - t)^{n+3}}{(n+2)(n+3)} \\ &+ \frac{\boldsymbol{C}_1 t_{\mathrm{f}}^{n+3}}{(n+2)(n+3)} + \frac{k(\boldsymbol{V}_{\mathrm{TMf}} - \boldsymbol{V}^*_{\mathrm{TMf}}) t_{\mathrm{f}}^{n+2}}{(n+1)(n+2)} \\ &- \frac{k(\boldsymbol{V}_{\mathrm{TMf}} - \boldsymbol{V}^*_{\mathrm{TMf}})(t_{\mathrm{f}} - t)^{n+2}}{(n+1)(n+2)} \end{aligned} \tag{24}$$

According to the final condition that $\boldsymbol{X}_{\mathrm{TMf}} = \boldsymbol{0}$, from Eq. (24), there is

$$\frac{t_f^{n+3}}{n+3}\boldsymbol{C}_1+\frac{kt_f^{n+2}}{n+2}\boldsymbol{V}_{TMf}=\boldsymbol{X}_{TM0}+\boldsymbol{V}_{TM0}t_f+\frac{1}{3}\boldsymbol{g}_{TM0}t_f^2+\frac{1}{n+2}k\boldsymbol{V}_{TMf}^{*}t_f^{n+2} \tag{25}$$

Additionally, when $t = t_f$, from Eq. (23), there is

$$\frac{t_f^{n+2}}{n+2}\boldsymbol{C}_1+\left(1+\frac{kt_f^{n+1}}{n+1}\right)\boldsymbol{V}_{TMf}=\boldsymbol{V}_{TM0}+\frac{1}{2}\boldsymbol{g}_{TM0}t_f+\frac{k}{n+1}\boldsymbol{V}_{TMf}^{*}t_f^{n+1} \tag{26}$$

Solving Eqs. (25) and (26) for $\boldsymbol{C}_1$ and $\boldsymbol{V}_{TMf}$ yields

$$\boldsymbol{C}_1=\boldsymbol{C}_2\Bigg/\left[\frac{t_f^{n+3}}{(n+3)}+\frac{kt_f^{2n+4}}{(n+1)(n+2)^2(n+3)}\right] \tag{27}$$

$$\boldsymbol{V}_{TMf}=\boldsymbol{C}_3\Bigg/\left[\frac{t_f}{(n+3)}+\frac{kt_f^{n+2}}{(n+1)(n+2)^2(n+3)}\right] \tag{28}$$

where

$$\begin{aligned}\boldsymbol{C}_2 &= \left(1+\frac{kt_f^{n+1}}{n+1}\right)\boldsymbol{X}_{TM0}+\left[1+\frac{kt_f^{n+1}}{(n+1)(n+2)}\right]\boldsymbol{V}_{TM0}t_f\\ &+\left[\frac{1}{3}+\frac{(1-n)kt_f^{n+1}}{6(n+1)(n+2)}\right]\boldsymbol{g}_{TM0}t_f^2+\frac{k}{n+2}\boldsymbol{V}_{TMf}^{*}t_f^{n+2}\end{aligned} \tag{29}$$

$$\begin{aligned}\boldsymbol{C}_3 &= -\frac{1}{(n+2)}\boldsymbol{X}_{TM0}-\frac{1}{(n+2)(n+3)}\boldsymbol{V}_{TM0}t_f\\ &+\frac{n\boldsymbol{g}_{TM0}t_f^2}{6(n+3)(n+2)}+\frac{k\boldsymbol{V}_{TMf}^{*}t_f^{n+2}}{(n+1)(n+3)(n+2)^2}\end{aligned} \tag{30}$$

Consider two cases: (1) $\boldsymbol{V}_{TMf}$ is unconstrained; (2) $\boldsymbol{V}_{TMf}$ is constrained.

(1) Optimal terminal guidance without constraint on $\boldsymbol{V}_{TMf}$

If $k = 0$, then $\boldsymbol{V}_{TMf}$ has no effect on the cost function and is thus unconstrained. Therefore, let $k = 0$ here. By substituting Eqs. (27) and (28) into Eq. (22) and letting $t = 0$, we obtain

$$\boldsymbol{a}_{M0}=\frac{(n+3)(\boldsymbol{X}_{TM0}+\boldsymbol{V}_{TM0}t_f)}{t_f^2}+\frac{n+3}{3}\boldsymbol{g}_{TM0} \tag{31}$$

(2) Optimal terminal guidance with constraint on $\boldsymbol{V}_{TMf}$

If one lets k go to positive infinity, then $\boldsymbol{V}_{TM}$ tends to $\boldsymbol{V}_{TMf}^{*}$ finally. Otherwise, the cost function would go to infinity. Use Eqs. (27) and (28) to calculate the following two limits related to $\boldsymbol{a}_M$.

$$\begin{aligned}\lim_{k\to\infty}\boldsymbol{C}_1 &= \frac{(n+2)^2(n+3)}{t_f^{n+3}}\boldsymbol{X}_{TM0}\\ &+\frac{(n+2)(n+3)}{t_f^{n+2}}\boldsymbol{V}_{TM0}+\frac{(n+2)(n+3)(1-n)}{6t_f^{n+1}}\boldsymbol{g}_{TM0}\\ &+\frac{(n+1)(n+2)(n+3)}{t_f^{n+2}}\boldsymbol{V}_{TMf}^{*}\end{aligned} \tag{32}$$

$$\begin{aligned}\lim_{k\to\infty}k(\boldsymbol{V}_{TMf}-\boldsymbol{V}_{TMf}^{*}) &= -\frac{(n+1)(n+2)(n+3)}{t_f^{n+2}}\boldsymbol{X}_{TM0}\\ &-\frac{(n+1)(n+2)}{t_f^{n+1}}\boldsymbol{V}_{TM0}+\frac{n(n+1)(n+2)}{6t_f^{n}}\boldsymbol{g}_{TM0}\\ &-\frac{(n+1)(n+2)^2}{t_f^{n+1}}\boldsymbol{V}_{TMf}^{*}\end{aligned} \tag{33}$$

By substituting Eqs. (32) and (33) into Eq. (22) and letting $t = 0$, we obtain

$$\begin{aligned}\boldsymbol{a}_{M0} &= \frac{(n+2)(n+3)}{t_f^2}\boldsymbol{X}_{TM0}+\frac{2(n+2)}{t_f}\boldsymbol{V}_{TM0}\\ &+\frac{(n+2)(3-n)}{6}\boldsymbol{g}_{TM0}+\frac{(n+1)(n+2)}{t_f}\boldsymbol{V}_{TMf}^{*}\end{aligned} \tag{34}$$

Note that the second term on the right side of Eq. (34) can be rewritten as

$$\frac{2(n+2)}{t_f}\boldsymbol{V}_{TM0}=\frac{(n+3)(n+2)}{t_f}\boldsymbol{V}_{TM0}-\frac{(n+1)(n+2)}{t_f}\boldsymbol{V}_{TM0} \tag{35}$$

To facilitate the subsequent derivation, by substituting Eq. (35) into Eq. (34), Eq. (34) can be rewritten as

$$\begin{aligned}\boldsymbol{a}_{M0} &= \frac{(n+2)(n+3)}{t_f^2}(\boldsymbol{X}_{TM0}+\boldsymbol{V}_{TM0}t_f)\\ &+\frac{(n+1)(n+2)}{t_f}(\boldsymbol{V}_{TMf}^{*}-\boldsymbol{V}_{TM0})+\frac{(n+2)(3-n)}{6}\boldsymbol{g}_{TM0}\end{aligned} \tag{36}$$

5. Flight time

As shown in Fig. 4, a non-rotating frame is created with origin at the center of mass of the missile and called frame F_M. Now we observe the motion of the target from frame F_M. If the missile flies without control, i.e. $\boldsymbol{a}_M = \boldsymbol{0}$, then the missile is only governed by gravity and will miss the target. For this case, the corresponding trajectory of the target in frame F_M is represented by the curve passing through the target and point P. Thereby, the ZEM is equal to the distance between the missile and point P. Denote the segment between the missile and point P as S_{MP}, and the segment between the missile and target as S_{MT}. The following explains that S_{MP} is perpendicular to S_{MT}. As shown in Fig. 5, since the engagement is outside the atmosphere, the missile uses the divert thrusters to perform lateral maneuvers in order to eliminate the ZEM, and uses the

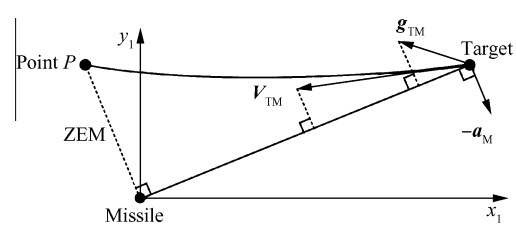

Fig. 4 ZEM prediction considering the effect of gravity.

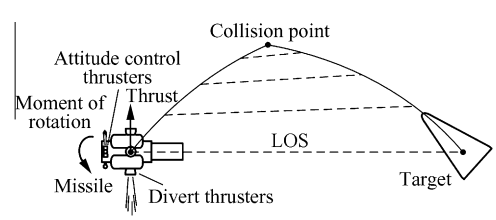

Fig. 5 Divert thrust is almost normal to LOS.

attitude control thrusters to adjust its attitude such that the longitudinal axis of the seeker always follows the LOS. Because the divert thrust is normal to the longitudinal axis which approximately coincides with the LOS, the divert thrust is approximately perpendicular to the LOS. Meanwhile, it is assumed that the direction of the LOS remains unchanged throughout the engagement. In fact, the LOS always rotates due to the effect of $\boldsymbol{g}_{\mathrm{TM}}$, even if the missile is just on a collision course. However, the angular displacement of LOS is very small, essentially because $\boldsymbol{g}_{\mathrm{TM}}$ is too small to result in a significant change in $\boldsymbol{V}_{\mathrm{TM}}$. The above analysis and assumption indicate that the displacement of the missile due to $\boldsymbol{a}_{\mathrm{M}}$ (i.e., the vector from the missile to the point P) is perpendicular to the initial LOS. Thereby, under these assumptions, the flight time t_{f} can be determined by analyzing the movement along the initial LOS.

Denote the components of $\boldsymbol{V}_{\mathrm{TM}}$ along and perpendicular to the initial LOS as $\boldsymbol{V}^{\mathrm{r}}_{\mathrm{TM}}$ and $\boldsymbol{V}^{\mathrm{n}}_{\mathrm{TM}}$, respectively, and denote the components of $\boldsymbol{g}_{\mathrm{TM}}$ along and perpendicular to the initial LOS as $\boldsymbol{g}^{\mathrm{r}}_{\mathrm{TM}}$ and $\boldsymbol{g}^{\mathrm{n}}_{\mathrm{TM}}$, respectively. Define $\hat{\boldsymbol{x}}_{\mathrm{TM}}$ as the unit vector of $\boldsymbol{X}_{\mathrm{TM}}$. $\hat{\boldsymbol{x}}_{\mathrm{TM0}}$ is the initial value of $\hat{\boldsymbol{x}}_{\mathrm{TM}}$. Let $R_{\mathrm{TM}} = \boldsymbol{X}_{\mathrm{TM}} \cdot \hat{\boldsymbol{x}}_{\mathrm{TM0}}, V^{\mathrm{r}}_{\mathrm{TM}} = \boldsymbol{V}_{\mathrm{TM}} \cdot \hat{\boldsymbol{x}}_{\mathrm{TM0}}$, and $g^{\mathrm{r}}_{\mathrm{TM}} = \boldsymbol{g}_{\mathrm{TM}} \cdot \hat{\boldsymbol{x}}_{\mathrm{TM0}}$. Note that since the missile always closes in the target, there is $V^{\mathrm{r}}_{\mathrm{TM}} < 0$.

Due to the assumption that the direction of the LOS remains unchanged, from Eq. (12), there is

$$g^{\mathrm{r}}_{\mathrm{TM}} = g^{\mathrm{r}}_{\mathrm{TM0}} \frac{t_{\mathrm{f}} - t}{t_{\mathrm{f}}} \tag{37}$$

where $g^{\mathrm{r}}_{\mathrm{TM0}}$ is the initial value of $g^{\mathrm{r}}_{\mathrm{TM}}$. Because it is assumed that $\boldsymbol{a}_{\mathrm{M}}$ does not affect the movement along the initial LOS, integrating the above equation yields

$$V^{\mathrm{r}}_{\mathrm{TM}} = V^{\mathrm{r}}_{\mathrm{TM0}} + \frac{1}{2} g^{\mathrm{r}}_{\mathrm{TM0}} t_{\mathrm{f}} - \frac{g^{\mathrm{r}}_{\mathrm{TM0}}}{2t_{\mathrm{f}}} (t_{\mathrm{f}} - t)^2 \tag{38}$$

where $V^{\mathrm{r}}_{\mathrm{TM0}}$ is the initial value of $V^{\mathrm{r}}_{\mathrm{TM}}$. Integrating the above equation yields

$$\begin{aligned} R_{\mathrm{TM}} &= R_{\mathrm{TM0}} + V^{\mathrm{r}}_{\mathrm{TM0}} t + \frac{1}{2} g^{r}_{\mathrm{TM0}} t_{\mathrm{f}} t \\ &\quad + \frac{g^{\mathrm{r}}_{\mathrm{TM0}}}{6t_{\mathrm{f}}} (t_{\mathrm{f}} - t)^3 - \frac{1}{6} g^{\mathrm{r}}_{\mathrm{TM0}} t_{\mathrm{f}}^2 \end{aligned} \tag{39}$$

where R_{TM0} is the initial value of R_{TM}. When $t = t_{\mathrm{f}}$, there is $R_{\mathrm{TMf}} = 0$, i.e.

$$R_{\mathrm{TM0}} + V^{\mathrm{r}}_{\mathrm{TM0}} t_{\mathrm{f}} + \frac{1}{3} g^{\mathrm{r}}_{\mathrm{TM0}} t_{\mathrm{f}}^2 = 0 \tag{40}$$

The above equation has two roots as

$$t_{\mathrm{f1}} = \frac{3}{2} \frac{\left(-V^{\mathrm{r}}_{\mathrm{TM0}} + \sqrt{\varDelta}\right)}{g^{\mathrm{r}}_{\mathrm{TM0}}}, t_{\mathrm{f2}} = \frac{3}{2} \frac{\left(-V^{\mathrm{r}}_{\mathrm{TM0}} - \sqrt{\varDelta}\right)}{g^{\mathrm{r}}_{\mathrm{TM0}}} \tag{41}$$

where

$$\varDelta = \left(V^{\mathrm{r}}_{\mathrm{TM0}}\right)^2 - \frac{4}{3} R_{\mathrm{TM0}} g^{\mathrm{r}}_{\mathrm{TM0}} \tag{42}$$

In practice, due to the careful planning of mission before launch, the engagement geometry generally meets the requirement for successful interception, i.e., the magnitude of $V^{\mathrm{r}}_{\mathrm{TM0}}$ is large enough to satisfy $\varDelta \geqslant 0$. To determine which root is the flight time and facilitates further derivation, the two roots are rewritten using a mathematical trick as follows:

$$\begin{aligned} t_{\mathrm{f1}} &= \frac{3}{2} \frac{\left(-V^{\mathrm{r}}_{\mathrm{TM0}} + \sqrt{\varDelta}\right)}{g^{\mathrm{r}}_{\mathrm{TM0}}} \frac{\left(-V^{\mathrm{r}}_{\mathrm{TM0}} - \sqrt{\varDelta}\right)}{\left(-V^{\mathrm{r}}_{\mathrm{TM0}} - \sqrt{\varDelta}\right)} \\ &= \frac{2R_{\mathrm{TM0}}}{-V^{\mathrm{r}}_{\mathrm{TM0}} - \sqrt{\varDelta}} \end{aligned} \tag{43}$$

and similarly,

$$t_{\mathrm{f2}} = \frac{2R_{\mathrm{TM0}}}{-V^{\mathrm{r}}_{\mathrm{TM0}} + \sqrt{\varDelta}} \tag{44}$$

Now determine which root is the flight time. According to Eq. (42), if $g^{\mathrm{r}}_{\mathrm{TM0}} \geqslant 0$, then $\varDelta \leqslant \left(V^{\mathrm{r}}_{\mathrm{TM0}}\right)^2$. Thus, it can be concluded from Eqs. (43) and (44) that $0 < t_{\mathrm{f2}} < t_{\mathrm{f1}}$. This means that at $t = t_{\mathrm{f2}}, R_{\mathrm{TM}} = 0$ is met for the first time. Therefore, the flight time is t_{f2}. If $g^{\mathrm{r}}_{\mathrm{TM0}} < 0$, then $\varDelta > \left(V^{\mathrm{r}}_{\mathrm{TM0}}\right)^2$. Substituting this into Eqs. (43) and (44), we obtain $t_{\mathrm{f1}} < 0 < t_{\mathrm{f2}}$. Thus, the flight time is still t_{f2}. All in all, the flight time is

$$t_{\mathrm{f}} = \frac{2R_{\mathrm{TM0}}}{-V^{\mathrm{r}}_{\mathrm{TM0}} + \sqrt{\varDelta}} \tag{45}$$

Using Eq. (45), the formulas of $\boldsymbol{a}_{\mathrm{M}}$ (Eqs. (31) and (36)) can be rewritten in terms of the angular velocity of LOS. Substituting Eq. (45) into an expression related to $\boldsymbol{a}_{\mathrm{M}}$ yields

$$\begin{aligned} &\frac{\boldsymbol{X}_{\mathrm{TM0}} + \boldsymbol{V}_{\mathrm{TM0}} t_{\mathrm{f}}}{t_{\mathrm{f}}^2} \\ &= \frac{\left(-V^{\mathrm{r}}_{\mathrm{TM0}} + \sqrt{\varDelta}\right)^2}{4R^2_{\mathrm{TM0}}} \boldsymbol{X}_{\mathrm{TM0}} + \frac{\left(-V^{\mathrm{r}}_{\mathrm{TM0}} + \sqrt{\varDelta}\right)}{2R_{\mathrm{TM0}}} \boldsymbol{V}_{\mathrm{TM0}} \\ &= \frac{\left(V^{\mathrm{r}}_{\mathrm{TM0}}\right)^2 - V^{\mathrm{r}}_{\mathrm{TM0}} \sqrt{\varDelta}}{2R^2_{\mathrm{TM0}}} \boldsymbol{X}_{\mathrm{TM0}} - \frac{g^{\mathrm{r}}_{\mathrm{TM0}}}{3R_{\mathrm{TM0}}} \boldsymbol{X}_{\mathrm{TM0}} \\ &+ \frac{\left(-V^{\mathrm{r}}_{\mathrm{TM0}} + \sqrt{\varDelta}\right)}{2R_{\mathrm{TM0}}} \boldsymbol{V}_{\mathrm{TM0}} \\ &= \frac{1}{2}\left(1 - \frac{\sqrt{\varDelta}}{V^{\mathrm{r}}_{\mathrm{TM0}}}\right) \times \\ &\frac{\left(V^{\mathrm{r}}_{\mathrm{TM0}}\right)^2 \boldsymbol{X}_{\mathrm{TM0}} - \left(V^{\mathrm{r}}_{\mathrm{TM0}} R_{\mathrm{TM0}}\right) \boldsymbol{V}_{\mathrm{TM0}}}{R^2_{\mathrm{TM0}}} - \frac{1}{3} \boldsymbol{g}^{\mathrm{r}}_{\mathrm{TM0}} \end{aligned} \tag{46}$$

Using some mathematical tricks that $\left(V^{\mathrm{r}}_{\mathrm{TM0}}\right)^2 = \boldsymbol{V}_{\mathrm{TM0}} \cdot \boldsymbol{V}^{\mathrm{r}}_{\mathrm{TM0}}, V^{\mathrm{r}}_{\mathrm{TM0}} R_{\mathrm{TM0}} = \boldsymbol{V}^{\mathrm{r}}_{\mathrm{TM0}} \cdot \boldsymbol{X}_{\mathrm{TM0}}$, and $R^2_{\mathrm{TM0}} = \boldsymbol{X}_{\mathrm{TM0}} \cdot \boldsymbol{X}_{\mathrm{TM0}}$, we obtain

$$\begin{aligned} &\frac{\boldsymbol{X}_{\mathrm{TM0}} + \boldsymbol{V}_{\mathrm{TM0}} t_{\mathrm{f}}}{t_{\mathrm{f}}^2} = \frac{1}{2}\left(1 - \frac{\sqrt{\varDelta}}{V^{\mathrm{r}}_{\mathrm{TM0}}}\right) \times \\ &\frac{\left(\boldsymbol{V}_{\mathrm{TM0}} \cdot \boldsymbol{V}^{\mathrm{r}}_{\mathrm{TM0}}\right) \boldsymbol{X}_{\mathrm{TM0}} - \left(\boldsymbol{V}^{\mathrm{r}}_{\mathrm{TM0}} \cdot \boldsymbol{X}_{\mathrm{TM0}}\right) \boldsymbol{V}_{\mathrm{TM0}}}{\boldsymbol{X}_{\mathrm{TM0}} \cdot \boldsymbol{X}_{\mathrm{TM0}}} - \frac{1}{3} \boldsymbol{g}^{\mathrm{r}}_{\mathrm{TM0}} \end{aligned} \tag{47}$$

Using the triple product expansion, i.e. $(\boldsymbol{a} \times \boldsymbol{b}) \times \boldsymbol{c} = (\boldsymbol{a} \cdot \boldsymbol{c})\boldsymbol{b} - (\boldsymbol{b} \cdot \boldsymbol{c})\boldsymbol{a}$, we obtain

$$\begin{aligned} &\frac{\boldsymbol{X}_{\mathrm{TM0}} + \boldsymbol{V}_{\mathrm{TM0}} t_{\mathrm{f}}}{t_{\mathrm{f}}^2} = \\ &-\frac{1}{2}\left(1 - \frac{\sqrt{\varDelta}}{V^{\mathrm{r}}_{\mathrm{TM0}}}\right) \boldsymbol{\omega}_{\mathrm{LOS0}} \times \boldsymbol{V}^{\mathrm{r}}_{\mathrm{TM0}} - \frac{1}{3} \boldsymbol{g}^{\mathrm{r}}_{\mathrm{TM0}} \end{aligned} \tag{48}$$

where $\boldsymbol{\omega}_{\mathrm{LOS}}$ is the angular velocity of LOS and its 3-D formula is

$$\boldsymbol{\omega}_{\mathrm{LOS}} = -\frac{\boldsymbol{V}_{\mathrm{TM}} \times \boldsymbol{X}_{\mathrm{TM}}}{\boldsymbol{X}_{\mathrm{TM}} \cdot \boldsymbol{X}_{\mathrm{TM}}} \tag{49}$$

In practice, $\boldsymbol{\omega}_{\mathrm{LOS}}$ is extracted from the data detected by the infrared seeker.[1,28,29] Substituting Eq. (45) into another expression related to $\boldsymbol{a}_{\mathrm{M}}$ yields

$$\frac{\boldsymbol{V}^{*}_{\mathrm{TMf}}-\boldsymbol{V}_{\mathrm{TM0}}}{t_{\mathrm{f}}}=-\frac{1}{2}\left(1-\frac{\sqrt{\Delta}}{V^{\mathrm{r}}_{\mathrm{TM0}}}\right)\times\frac{(\boldsymbol{X}_{\mathrm{TM}}\cdot\boldsymbol{V}_{\mathrm{TM}})(\boldsymbol{V}^{*}_{\mathrm{TMf}}-\boldsymbol{V}_{\mathrm{TM0}})}{\boldsymbol{X}_{\mathrm{TM}}\cdot\boldsymbol{X}_{\mathrm{TM}}} \tag{50}$$

Using Eqs. (48) and (50), the OTG laws can be expressed in terms of the angular velocity of LOS, as follows:

(1) Optimal terminal guidance without constraint on $\boldsymbol{V}_{TMf}$

Substituting Eq. (48) into Eq. (31) yields

$$\boldsymbol{a}_{\mathrm{M0}}=-\frac{n+3}{2}\left(1-\frac{\sqrt{\Delta}}{V^{\mathrm{r}}_{\mathrm{TM0}}}\right)\boldsymbol{\omega}_{\mathrm{LOS0}}\times\boldsymbol{V}^{\mathrm{r}}_{\mathrm{TM0}}+\frac{n+3}{3}\boldsymbol{g}^{\mathrm{n}}_{\mathrm{TM0}} \tag{51}$$

(2) Optimal terminal guidance with constraint on $\boldsymbol{V}_{\mathrm{TMf}}$

Substituting Eqs. (48) and (50) into Eq. (36) yields

$$\boldsymbol{a}_{\mathrm{M0}}=(n+2)(n+3)\times\left[-\frac{1}{2}\left(1-\frac{\sqrt{\Delta}}{V^{\mathrm{r}}_{\mathrm{TM0}}}\right)\boldsymbol{\omega}_{\mathrm{LOS0}}\times\boldsymbol{V}^{\mathrm{r}}_{\mathrm{TM0}}+\frac{1}{3}\boldsymbol{g}^{\mathrm{n}}_{\mathrm{TM0}}\right]+(n+1)(n+2)\left[-\frac{1}{2}\left(1-\frac{\sqrt{\Delta}}{V^{\mathrm{r}}_{\mathrm{TM0}}}\right)\times\frac{(\boldsymbol{X}_{\mathrm{TM0}}\cdot\boldsymbol{V}_{\mathrm{TM0}})(\boldsymbol{V}^{*}_{\mathrm{TMf}}-\boldsymbol{V}_{\mathrm{TM0}})}{\boldsymbol{X}_{\mathrm{TM0}}\cdot\boldsymbol{X}_{\mathrm{TM0}}}-\frac{1}{2}\boldsymbol{g}_{\mathrm{TM0}}\right] \tag{52}$$

Because $V^{\mathrm{r}}_{\mathrm{TM0}}<0$, there is

$$-\frac{\sqrt{\Delta}}{V^{\mathrm{r}}_{\mathrm{TM0}}}=\sqrt{1-\frac{4}{3}\frac{R_{\mathrm{TM0}}g^{\mathrm{r}}_{\mathrm{TM0}}}{\left(V^{\mathrm{r}}_{\mathrm{TM0}}\right)^{2}}} \tag{53}$$

If $R_{\mathrm{TM}}g^{\mathrm{r}}_{\mathrm{TM}}/(V^{\mathrm{r}}_{\mathrm{TM}})^{2}\approx 0$, the formulas of $\boldsymbol{a}_{\mathrm{M}}$ can be further simplified by assuming that $-\sqrt{\Delta}/V^{\mathrm{r}}_{\mathrm{TM0}}\approx 1$.

In practice, the guidance command is generated in real time by substituting the current states of motion into Eq. (51) or Eq. (52).

Note that Eqs. (51) and (52) are more suitable for practice than Eqs. (31) and (36); because (1) due to the help of the infrared seeker, the estimation accuracy of the angular velocity of LOS is much higher than that of the remaining flight time (i.e. time to go), especially when the missile is very close to the target; (2) since the time to go appears in the denominators of the guidance formulas, the miss distance is highly sensitive to the estimation error of the time-to-go, especially if there is a bias error in the estimated time-to-go.[1,30] In addition, because $\boldsymbol{X}_{\mathrm{TM0}}$ also appears in a denominator of Eq. (52), if there is a measurement error of the relative position, it can result in a waste of fuel and may even cause the missile to miss the target. Section 6.2 gives an example to show the influence of the measurement error.

In Ref.[1], Zarchan demonstrated that the 2D PN expressed in terms of ZEM and t_{go} is equivalent to that expressed in terms of the angular rate of LOS by geometrically analyzing the relationship between ZEM and the angular rate of LOS. Different from Ref.[1], the transformation method presented here is proposed for 3D guidance laws and based on vector operations, rather than geometric analysis. Additionally, the consideration of gravity greatly increases the difficulty of transformation and causes the method presented in Ref.[1] to fail to handle the OTG cases.

6. Results and discussion

6.1. OTG without constraint on $\boldsymbol{V}_{TMf}$

In this subsection, some examples are given where $\boldsymbol{V}_{\mathrm{TMf}}$ is unconstrained. In these examples, the simulation results of OTG are compared with that of PN, APN, and PG. The commands of OTG, PN, and APN can be expressed uniformly as

$$\boldsymbol{a}_{\mathrm{M}}=-N_1\boldsymbol{\omega}_{\mathrm{LOS}}\times\boldsymbol{V}^{\mathrm{r}}_{\mathrm{TM}}+N_2\boldsymbol{g}^{\mathrm{n}}_{\mathrm{TM}} \tag{54}$$

where for PN, $N_1=3+n$ and $N_2=0$. For APN, $N_1=3+n$ and $N_2=(3+n)/2$. For OTG, $N_1=0.5(n+3)\times\left(1-\sqrt{\Delta}/V^{\mathrm{r}}_{\mathrm{TM}}\right)$ and $N_2=(3+n)/3$.

Here, the guidance parameter $n\geqslant 0$. The command of PG can be expressed as

$$\boldsymbol{a}_{\mathrm{M}}=\frac{N_1\boldsymbol{X}_{\mathrm{ZEM}}}{t^{2}_{\mathrm{go}}} \tag{55}$$

where $N_1=3+n$ and $\boldsymbol{X}_{\mathrm{ZEM}}$ is the zero-effort miss vector. In each guidance cycle of PG, the onboard computer lets $\boldsymbol{a}_{\mathrm{M}}=\boldsymbol{0}$ and then integrates Eqs. (1)–(4) numerically. When $\boldsymbol{X}_{9m}\cdot\boldsymbol{V}_{\mathrm{TM}}=\boldsymbol{0}$, the simulation stops. Then, let t_{go} be equal to the stop time and let $\boldsymbol{X}_{\mathrm{ZEM}}$ be equal to the value of $\boldsymbol{X}_{\mathrm{TM}}$ at the stop time. PG uses the component of $\boldsymbol{a}_{\mathrm{M}}$ perpendicular to the LOS as the guidance command.

Consider two cases about the PIP here: **Case 1.** the PIP has no error; **Case 2.** the PIP has an error of about 50 km.

In Case 1, the initial states of the KKV are $\boldsymbol{X}_{\mathrm{M0}}=[786280.91,\ -1300973.39,\ 7286277.30]^{\mathrm{T}}$ m and $\boldsymbol{V}_{\mathrm{M0}}=[2837.72,\ 5409.49,\ 1553.36]^{\mathrm{T}}$ m/s, and the initial states of the target are $\boldsymbol{X}_{\mathrm{T0}}=[981407.04,\ -861312.60,\ 7722585.39]^{\mathrm{T}}$ m and $\boldsymbol{V}_{\mathrm{T0}}=[1725.21,\ -6831.13,\ -976.11]^{\mathrm{T}}$ m/s. In this case, let $n=0$ for all the four guidance laws. Define the velocity increment ΔV as

$$\Delta V(t)=\int_0^t ||\boldsymbol{a}_M||\mathrm{d}t \tag{56}$$

Because the thrust acceleration is proportional to the mass flow rate of fuel, ΔV reflects the fuel consumption.

The simulation results are shown in Table 1 and Figs. 6–9. As can be seen from Table 1, PG consumes the least fuel, but requires the heaviest computational load. The velocity increment of OTG is almost as small as that of PG, but the computing time of OTG is much shorter than that of PG. Additionally, the velocity increment of APN is almost half that of PN. Fig. 6 shows the trajectories and the corresponding

Table 1 Comparisons of simulation results in Case 1.

Guidance law	ΔV (m/s)	Computing time (s)
OTG	1.032	0.0844
PN	91.510	0.0813
APN	46.950	0.0744
PG	0	12.7356

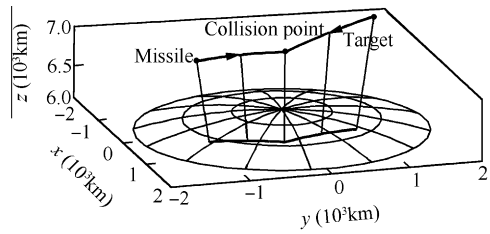

Fig. 6 Engagement trajectories for OTG in Case 1.

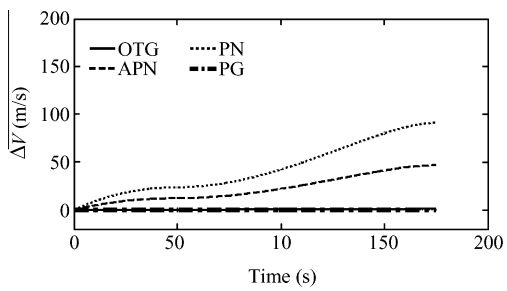

Fig. 7 Histories of velocity increments in Case 1.

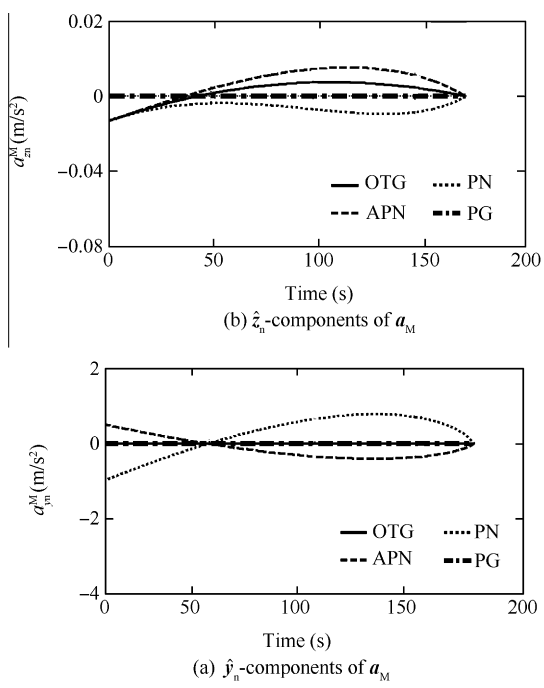

Fig. 8 Histories of guidance commands in Case 1.

ground tracks of the missile and target for OTG. Because the trajectories for the four guidance laws are nearly coincident and not easily distinguishable, only the trajectories for OTG are presented here. Fig. 7 shows the histories of the velocity increments for all the guidance laws. Define plane P_{EMT} as the plane containing the Earth center, missile, and target. Define $\hat{\boldsymbol{y}}_n$ as the unit vector that is perpendicular to the current LOS in plane P_{EMT} and has a positive projection on $\boldsymbol{X}_{\mathrm{M}}$. Define $\hat{\boldsymbol{z}}_{\mathrm{n}}$ as the unit vector perpendicular to plane P_{EMT} and determined by $\hat{\boldsymbol{z}}_{\mathrm{n}} = \hat{\boldsymbol{x}}_{\mathrm{TM}} \times \hat{\boldsymbol{y}}_{\mathrm{n}}$. Fig. 8(a) shows the histories of the components of $\boldsymbol{a}_{\mathrm{M}}$ along $\hat{y}_{\mathrm{n}}$, denoted as $a_{y\mathrm{n}}^{\mathrm{M}}$. Fig. 8(b) shows

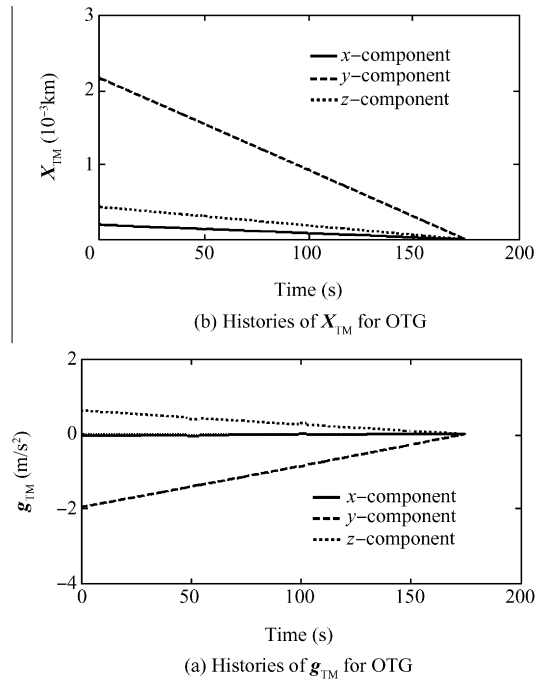

Fig. 9 Histories of $\boldsymbol{g}_{\mathrm{TM}}$ and $\boldsymbol{X}_{\mathrm{TM}}$ for OTG in Case 1.

Table 2 Comparisons of simulation results in Case 2.

Guidance law	ΔV (m/s)	Computing time (s)
OTG	230.93	0.1636
PN	399.67	0.1628
APN	292.87	0.1730
PG	232.60	42.7442

the histories of the components of $\boldsymbol{a}_{\mathrm{M}}$ along $\hat{\boldsymbol{z}}_{\mathrm{n}}$, denoted as $a_{z\mathrm{n}}^{\mathrm{M}}$. From Fig. 8, it can be seen that due to the use of inaccurate gravity models, PN and APN cause the missiles to perform unnecessary maneuvers and thus result in an apparent waste of fuel. Fig. 9 shows the histories of $\boldsymbol{g}_{\mathrm{TM}}$ and $\boldsymbol{X}_{\mathrm{TM}}$ for OTG. Here, it can be seen that both $\boldsymbol{g}_{\mathrm{TM}}$ and $\boldsymbol{X}_{\mathrm{TM}}$ vary almost linearly with time. Fig. 9(b) indicates that the direction of LOS is almost unchanged during the interception.

Now Case 2 is considered where there is a large PIP error of about 50 km in the beginning. To show the influence of the initial distance on the linearity of the gravity difference, the initial separation is enlarged to about 4000 km. The initial conditions are $\boldsymbol{X}_{\mathrm{M0}} = [192442.95, -2085138.26, 6726394.99]^{\mathrm{T}}$ m, $\boldsymbol{V}_{\mathrm{M0}} = [3418.94, 5190.08, 3269.23]^{\mathrm{T}}$ m/s, $\boldsymbol{X}_{\mathrm{T0}} = [569875.90, 1928987.06, 7526018.77]^{\mathrm{T}}$ m, and $\boldsymbol{V}_{\mathrm{T0}} = [2262.74, -6806.83, 834.46]^{\mathrm{T}}$ m/s. In this case, the parameter n of the four guidance laws is set to 1. The simulation results are shown in Table 2 and Figs. 10–13. From Table 2, it can be seen that the velocity increments for OTG and PG are still significantly smaller than the other two, but the computing time for PG is much longer than the others. Also because the trajectories for the four guidance laws are very similar, Fig. 10 only shows the trajectories and the corresponding ground tracks for OTG. Fig. 11 shows the histories of the velocity increments. Fig. 12 shows the histories of the acceleration commands for the four guidance laws. As can be seen from Fig. 12(a), in PN, because the effect

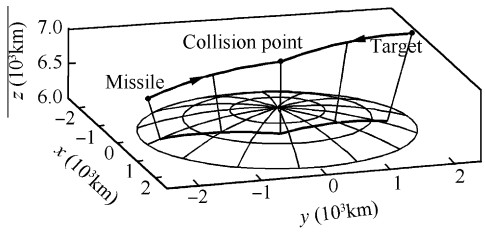

Fig. 10 Engagement trajectories for OTG in Case 2.

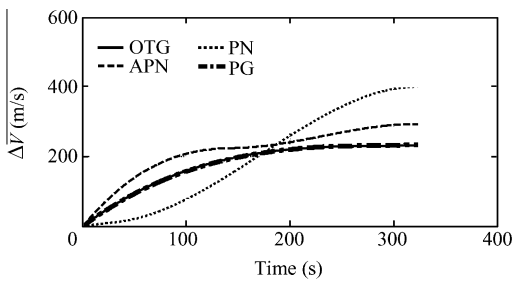

Fig. 11 Histories of velocity increments in Case 2.

of $\boldsymbol{g}_{\mathrm{TM}}$ is not considered, the ZEM is underestimated and thus the commanded acceleration is insufficient in the beginning, which results in a large lateral divert requirement in the latter part of the trajectory. On the contrary, APN overestimates the ZEM since it assumes that $\boldsymbol{g}_{\mathrm{TM}}$ is constant throughout the remaining flight and equal to the current value. Therefore, the maneuvering acceleration is too large in the beginning. This causes that the missile has to change the direction of thrust to the opposite in the latter part of the flight. By contrast, OTG estimates the ZEM accurately and thus control the missile to perform proper maneuvers. Therefore, as shown in Fig. 11, OTG requires much smaller velocity increment than PN and APN. From Fig. 13, it can be seen that although the initial separation is up to 4000 km, $\boldsymbol{g}_{\mathrm{TM}}$ and $\boldsymbol{X}_{\mathrm{TM}}$ still vary almost linearly with time.

Define R_{TGP} as the distance at which the terminal guidance phase starts. Now observe how R_{TGP} influences the velocity increments of PN, APN, and OTG. In the simulations conducted here, there are two flight phases. The first phase is the coast phase where the missile is only governed by gravity and thus flies along a ballistic trajectory. When the distance between the missile and target reduces to R_{TGP}, the terminal guidance phase begins. Here, two cases about the coast phase are considered: (1) the missile is just on a collision course, which means that there is no PIP error, and (2) the trajectory of the missile has a PIP error of about 5 km. By setting R_{TGP} to different values and then conducting a large number of simulations, the profiles of the velocity increments with respect to R_{TGP} can be obtained, as shown in Fig. 14. Here, Fig. 14(a) shows the profiles corresponding to the case without PIP error, and Fig. 14(b) shows the profiles corresponding to the case with PIP error. As shown in Fig. 14(a), it can be seen that OTG has very high fuel efficiency, compared with PN and APN. This figure also shows that the amount of the waste fuel for APN is about half that for PN. As shown in Fig. 14(b), shorter R_{TGP} tends to increase the required heading correction and thus increase the lateral divert requirement. Inversely, for OTG, longer R_{TGP} tends to reduce the lateral divert requirement significantly. However, because PN and APN adopt the inaccurate gravity models and thus cause the missile to perform unnecessary maneuvers, longer R_{TGP} tends to increase the lateral divert requirements for PN and APN.

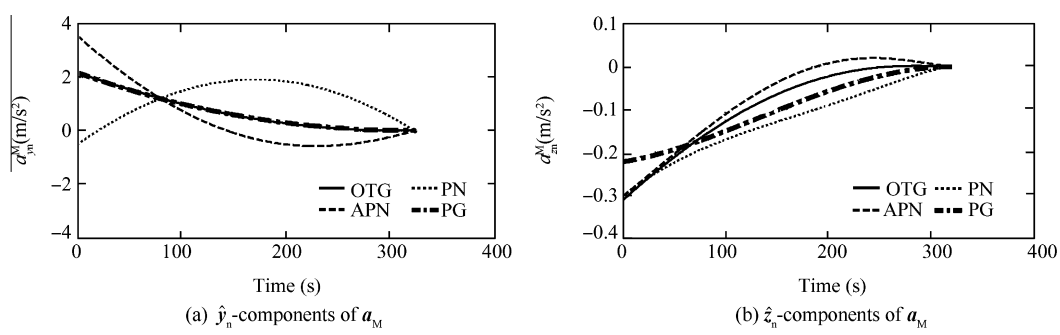

(a) $\hat{y}_{\mathrm{n}}$-components of $\boldsymbol{a}_{\mathrm{M}}$ (b) $\hat{z}_{\mathrm{n}}$-components of $\boldsymbol{a}_{\mathrm{M}}$

Fig. 12 Histories of the guidance commands in Case 2.

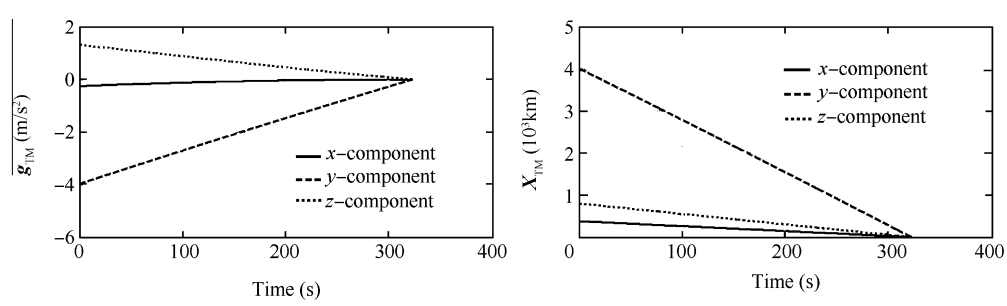

(a) Histories of $\boldsymbol{g}_{\mathrm{TM}}$ for OTG (b) Histories of $\boldsymbol{X}_{\mathrm{TM}}$ for OTG

Fig. 13 Histories of $\boldsymbol{g}_{\mathrm{TM}}$ and $\boldsymbol{X}_{\mathrm{TM}}$ for OTG in Case 2.

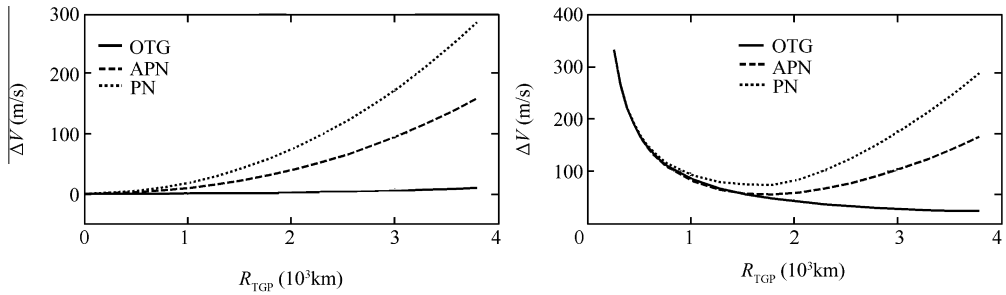

(a) Case without PIP error (b) Case with PIP error

Fig. 14 Profiles of ΔV versus R_{TGP}.

6.2. OTG with constraint on V_{TMf}

Now consider the cases with constraint on $\boldsymbol{V}_{TMf}$, where it is desired that the missile collides head-on with the target. As a comparison, the results of generalized vector explicit guidance (GENEX)[17] are also given here. Although GENEX is originally expressed in terms of ZEM and t_{go}, using the transformation method shown in Section 5, GENEX can also be reformulated in terms of the angular velocity of LOS as follows:

$$\boldsymbol{a}_M = -(n+2)(n+3)\boldsymbol{\omega}_{LOS} \times \boldsymbol{V}_{TM}^r - (n+1)(n+2)\frac{(\boldsymbol{X}_{TM}\cdot\boldsymbol{V}_{TM})(\boldsymbol{V}_{TMf}^* - \boldsymbol{V}_{TM})}{\boldsymbol{X}_{TM}\cdot\boldsymbol{X}_{TM}} \tag{57}$$

The parameter n appearing in Eqs. (52) and (57) is set to be 1. Before launching the missile, the command and control center can figure out the position of the PIP and the velocity vector of the target at the PIP, where the unit vector of the velocity vector of the target at the PIP is denoted as $\hat{\boldsymbol{v}}_{Tf}$. Then, for a head-on collision, let the desired final relative velocity vector be

$$\boldsymbol{V}_{TMf}^* = ||\boldsymbol{V}_{TM}||\hat{\boldsymbol{v}}_{Tf} \tag{58}$$

A scenario is considered here that although the intercept trajectory has been planned perfectly with $\hat{\boldsymbol{v}}_{Tf} = [-0.1840, -0.9720, -0.1462]^T$, due to the guidance error at the boost phase, the missile has a heading error of about 0.5° at the beginning of the terminal guidance phase. For this scenario, at the terminal guidance phase, the initial conditions are $\boldsymbol{X}_{M0} = [354390.76, -1468209.45, 6924581.65]^T$ m, $\boldsymbol{V}_{M0} = [1142.97, 4964.53, 2714.43]^T$ m/s, $\boldsymbol{X}_{T0} = [942888.61, 1633401.66, 7406664.03]^T$ m, and $\boldsymbol{V}_{T0} = [-1168.38, -6981.35, 680.63]^T$ m/s.

To show the influence of the measurement error of $\boldsymbol{X}_{TM}$ on OTG, an additional case is considered where it is assumed that the measured magnitude of $\boldsymbol{X}_{TM}$ is 100 m less than its real value and OTG is used as control.

The simulation results are shown in Table 3 and Figs. 15–17, where the solid lines represent the ideal results of OTG, the dashed lines represent the ideal results of GENEX, and the dotted lines represent the results of the case with the measurement error of $\boldsymbol{X}_{TM}$. As can be seen from Table 3, the velocity increment of OTG is about half that of GENEX, and the measurement error of $\boldsymbol{X}_{TM}$ leads to more fuel consumption. Also because the trajectories for the three cases are very similar, Fig. 15 only shows the trajectories and the corresponding ground tracks for OTG. Define θ as the angle between the velocity vectors of the missile and target. Fig. 16 shows the histories of ΔV and θ. From Fig. 16(a), it can also be seen that the velocity increment of OTG is much smaller than that of GENEX. From Fig. 16(b), it can be seen that θ goes to 180° finally, which means that the missile hits the target from the head-on direction. As can be seen from Fig. 17(a), because GENEX does not consider the effect of gravity, GENEX causes the missile to perform some unnecessary maneuvers and thus results in a waste of fuel. In Fig. 17(b), because $\boldsymbol{g}_{TM}$ has no component along $\hat{z}_n$, OTG and GENEX are almost the same in this direction and thus generate the similar acceleration commands. In the case with measurement error of $\boldsymbol{X}_{TM}$, when the missile is close enough to the target where the distance between them is within hundreds of meters, the measurement error results in rapid changes in the guidance command, which leads to fuel waste and a large error in θ.

Table 3 Comparisons of simulation results with constraint on $\boldsymbol{V}_{TMf}$.

Case	ΔV (m/s)	Computing time (s)
OTG	83.66	0.1469
GENEX	164.58	0.1201
Case with measurement error	104.33	0.1571

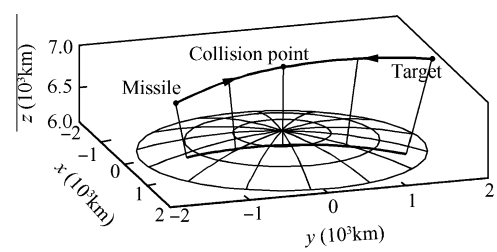

Fig. 15 Engagement trajectories for OTG with constraint on $\boldsymbol{V}_{TMf}$.

6.3. Improved pulsed guidance

An example is given here to show that some achievements of this paper can be used to improve the fuel efficiency of the pulsed guidance law employed by the missile with fixed thrust level.

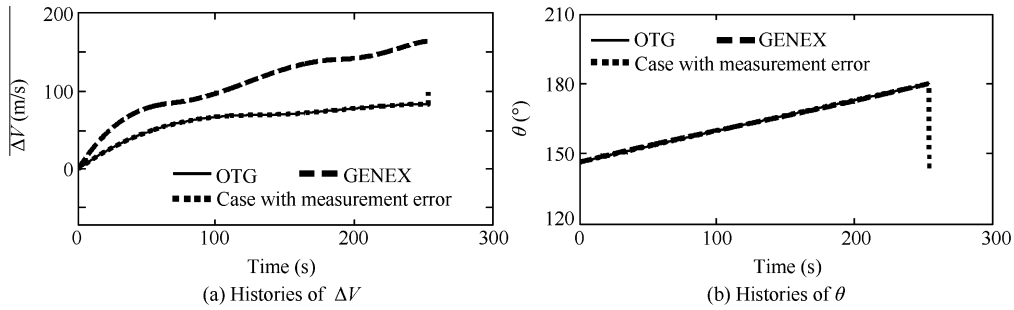

(a) Histories of ΔV (b) Histories of θ

Fig. 16 Histories of ΔV and θ for the cases with constraint on V_{TMf}.

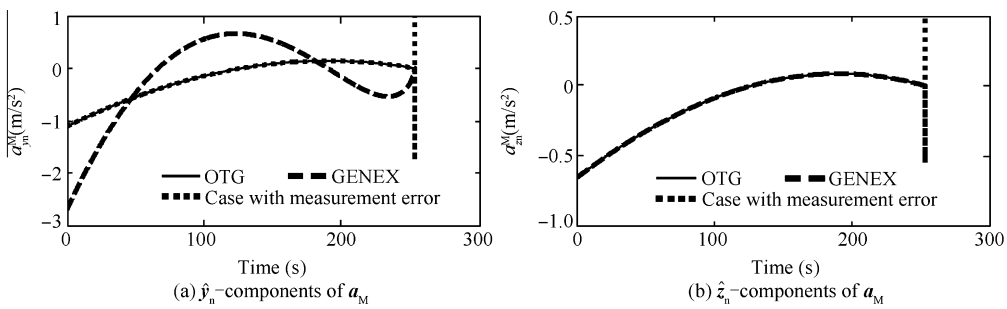

(a) $\hat{y}_{\mathrm{n}}$–components of $\boldsymbol{a}_{\mathrm{M}}$ (b) $\hat{z}_{\mathrm{n}}$–components of $\boldsymbol{a}_{\mathrm{M}}$

Fig. 17 Histories of guidance commands for the cases with constraint on V_{TMf}.

Zarchan introduced a 2D pulsed guidance law and demonstrated its performance in the long-range exoatmospheric interception.[1] Here, the guidance is extended to a 3D one and called the basic pulsed guidance (BPG) law. In general, KKV has four divert thrusters in a cruciform configuration. Assume that the axis of a pair of coaxial thrusters remains along $\hat{\boldsymbol{y}}_{\mathrm{n}}$, while the axis of the other pair of coaxial thrusters remains along $\hat{\boldsymbol{z}}_{\mathrm{n}}$. The components of $\boldsymbol{X}_{\mathrm{ZEM}}$ along $\hat{\boldsymbol{y}}_{\mathrm{n}}$ and $\hat{\boldsymbol{z}}_{\mathrm{n}}$ are denoted as $\boldsymbol{X}_{\mathrm{yn}}^{\mathrm{ZEM}}$ and $\boldsymbol{X}_{\mathrm{zn}}^{\mathrm{ZEM}}$, respectively.

As shown in Fig. 18, if there is a guidance pulse of magnitude a_{M} lasting for Δt seconds, then the profile of the lateral maneuvering speed ΔV consists of two segments. In such a case, the lateral maneuvering range is equal to the area of the region enclosed by the time axis and lines depicted in Fig. 18(b).

As the guidance tries to remove the predicted ZEM using one pulse, let the displacement due to thrust be equal to the predicted $\boldsymbol{X}_{\mathrm{ZEM}}$ as

$$||\boldsymbol{X}_{\mathrm{yn}}^{\mathrm{ZEM}}|| = 0.5a_{\mathrm{M}}\Delta t_{\mathrm{yn}}^2 + a_{\mathrm{M}}\Delta t_{\mathrm{yn}}(t_{\mathrm{go}} - \Delta t_{\mathrm{yn}}) \tag{59}$$

$$||\boldsymbol{X}_{\mathrm{zn}}^{\mathrm{ZEM}}|| = 0.5a_{\mathrm{M}}\Delta t_{\mathrm{zn}}^2 + a_{\mathrm{M}}\Delta t_{\mathrm{zn}}(t_{\mathrm{go}} - \Delta t_{\mathrm{zn}}) \tag{60}$$

Here, Δt_{yn} is the commanded duration time for the thrust with the same direction as $\boldsymbol{X}_{\mathrm{yn}}^{\mathrm{ZEM}}$ and Δt_{zn} the commanded duration time for the thrust with the same direction as $\boldsymbol{X}_{\mathrm{zn}}^{\mathrm{ZEM}}$. Solving the above two equations, we obtain

$$\Delta t_{\mathrm{yn}} = t_{\mathrm{go}} - \sqrt{t_{\mathrm{go}}^2 - \frac{2||\boldsymbol{X}_{\mathrm{yn}}^{\mathrm{ZEM}}||}{a_{\mathrm{M}}}} \tag{61}$$

$$\Delta t_{\mathrm{zn}} = t_{\mathrm{go}} - \sqrt{t_{\mathrm{go}}^2 - \frac{2||\boldsymbol{X}_{\mathrm{zn}}^{\mathrm{ZEM}}||}{a_{\mathrm{M}}}} \tag{62}$$

According to Ref.[1], in BPG, $\boldsymbol{X}_{\mathrm{ZEM}}$ and t_{go} are predicted by

$$\boldsymbol{X}_{\mathrm{ZEM}} = \boldsymbol{X}_{\mathrm{TM}} + \boldsymbol{V}_{\mathrm{TM}}t_{\mathrm{go}} \tag{63}$$

$$t_{\mathrm{go}} = -R_{\mathrm{TM}}/V_{\mathrm{TM}}^{\tau} \tag{64}$$

Table 4 Comparisons of simulation results for BPG and IPG.

Guidance law	Miss distance (m)	ΔV (m/s)	Computing time (s)
IPG	0.1840	204.91	0.7005
BPG	0.2992	425.69	0.6527

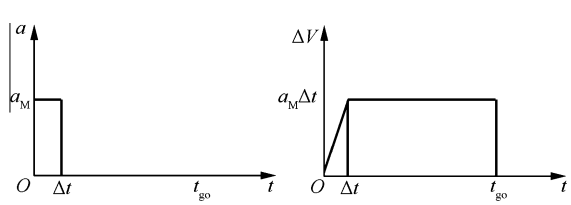

Fig. 18 Sketch map of pulsed guidance.

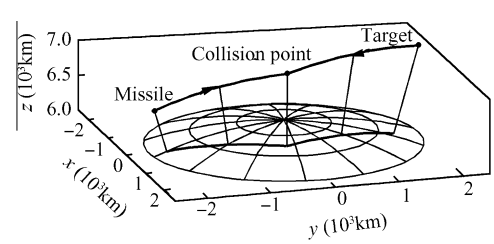

Fig. 19 Engagement trajectories for IPG.

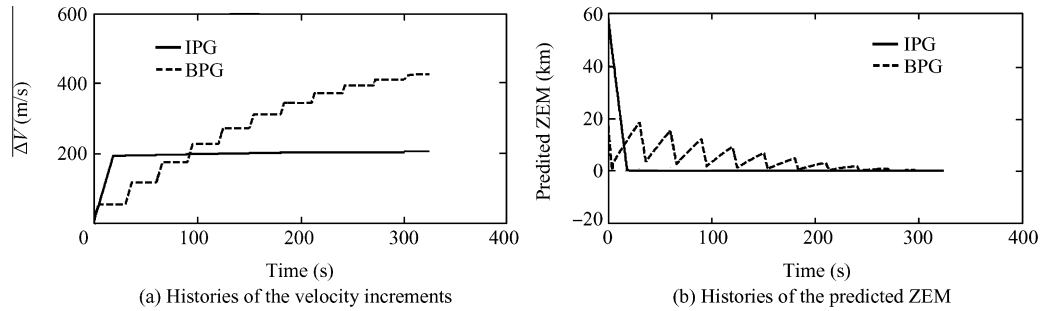

Fig. 20 Histories of ΔV and predicted ZEM for IPG and BPG.

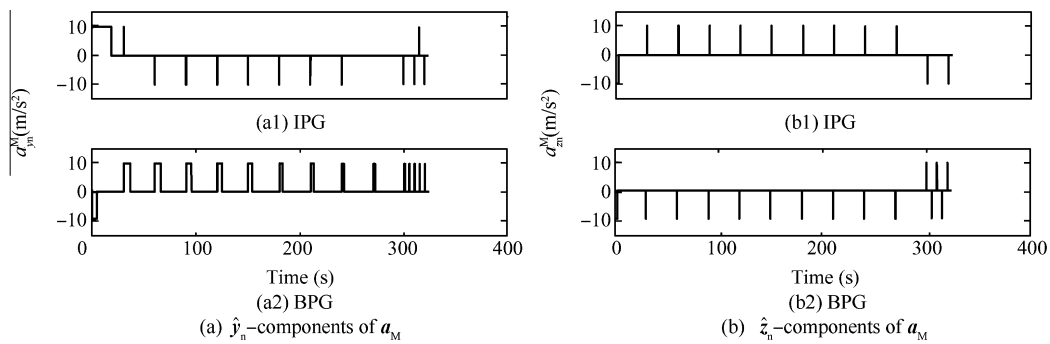

Fig. 21 Histories of guidance commands for IPG and BPG.

Note again that $V_{TM}^{\tau} < 0$. Because the above prediction formulas are inaccurate due to the ignorance of gravity, one trajectory correction cannot eliminate all the real ZEM. Therefore, more trajectory corrections are needed. In Ref.[1], these corrections are distributed at equal intervals during the flight. To reduce the miss distance, this scheme is slightly modified as: when $t_{go} > 30$ s, the trajectory correction is conducted every 30 s, but when $t_{go} \leqslant 30$ s, the trajectory correction is conducted every 5 s.

Using some achievements of this paper, the prediction formulas of $\boldsymbol{X}_{ZEM}$ and t_{go} considering the effect of gravity can be obtained. From Ref.[1], there is $\boldsymbol{a}_M = N_1 \boldsymbol{X}_{ZEM}/t_{go}^2$ where $N_1 = 3 + n$. By comparing this with Eq. (31), we obtain

$$\boldsymbol{X}_{ZEM} = \boldsymbol{X}_{TM} + \boldsymbol{V}_{TM} t_{go} + \frac{1}{3}\boldsymbol{g}_{TM} t_{go}^2 \tag{65}$$

From Eq. (45), there is

$$t_{go} = \frac{2R_{TM}}{-V_{TM}^{\tau} + \sqrt{\Delta}} \tag{66}$$

where $\Delta = (V_{TM}^{\tau})^2 - (4/3)R_{TM}g_{TM}^{r}$. The modified guidance is called the improved pulsed guidance (IPG) law. In fact, because the fuel consumption leads to a reduction in mass, the thrust acceleration level a_M increases gradually during the flight. However, for simplicity, assume that a_M is a constant because the change in a_M is small, and has a value of 10 m/s.[2]

The initial conditions for the current case are the same as those for Case 2 in Section 6.1. The simulation results are shown in Table 4 and Figs. 19–21. As can be seen from Table 4 and Fig. 20(a), because IPG gives full consideration to the effect of gravity, its miss distance and velocity increment are much smaller than those of BPG. In Fig. 19, only the trajectories and the corresponding ground tracks for IPG are presented, also because the trajectories for IPG and BPG are very similar. As shown in Fig. 20(b), because IPG predicts the ZEM accurately and controls the missile to perform lateral maneuvers properly, the predicted ZEM of IPG remains nearly zero after the first trajectory correction. Fig. 21 shows the histories of the lateral maneuvering accelerations.

7. Conclusions

In this paper, using optimal control theory, two optimal terminal guidance laws are developed for exoatmospheric interception: one considers the final velocity vector constraint, whereas the other does not consider it. Because the developed guidance laws give full consideration to the effect of gravity and need not conduct any onboard trajectory simulation, the new guidance laws consume much less fuel than the traditional guidance laws while demanding a light computational load. To convert the OTG laws expressed in terms of $\boldsymbol{X}_{TM}$, $\boldsymbol{V}_{TM}$ and t_{go} into that expressed in terms of $\boldsymbol{\omega}_{LOS}$, the 3D transformation method based on vector operations is proposed, which considers the effect of the gravity difference, especially on the flight time. Additionally, an example is given to show that if the prediction formulas of $\boldsymbol{X}_{ZEM}$ and t_{go} proposed in this study are applied to the pulsed guidance law, the fuel efficiency of the guidance law can be significantly improved. Different from PN, the implement of the OTG laws requires the information on the positions of the missile and target in order to calculate the gravity difference and guidance coefficients.

References

1. Zarchan P. *Tactical and strategic missile guidance*. 6th ed. Virginia: AIAA Progress in Aeronautics and Astronautics; 2012. p. 299–323.
2. Yuan CL. Homing and navigation courses of automatic target-seeking devices. *J Appl Phys* 1948;**19**(12):1122–8.
3. Adler FP. Missile guidance by three-dimensional proportional navigation. *J Appl Phys* 1956;**27**(5):500–7.
4. Bryson AE, Ho YC. *Applied optimal control*. Waltham: Blaisdell; 1969. p. 148–76.
5. Guelman M. The closed-form solution of true proportional navigation. *IEEE Trans Aerosp Electron Syst* 1976;**12**(5):472–82.
6. Becker K. Closed-form solution of pure proportional navigation. *IEEE Trans Aerosp Electron Syst* 1990;**26**(3):526–33.
7. Yu WB, Chen WC. Guidance law with circular no fly zone constraint. *Nonlinear Dyn* 2014;**78**(3):1953–71.
8. Yang CD, Yang CC. Analytical solution of generalized 3D proportional navigation. In: *Proceedings of the 34th conference on decision & control;* 1995 December 13-15; New Orleans, LA, USA. Piscataway. NJ: IEEE Press; 1995. p. 3974–9.
9. Yang CD. Analytical solution of 3D true proportional navigation. *IEEE Trans Aerosp Electron Syst* 1996;**32**(4):1510–22.
10. Li K, Zhang T, Chen L. Ideal proportional navigation for exoatmospheric interception. *Chin J Aeronaut* 2013;**26**(4):976–85.
11. Su WS, Yao DN, Li KB, Chen L. A novel biased proportional navigation guidance law for close approach phase. *Chin J Aeronaut* 2016;**29**(1):228–37.
12. Garber V. Optimum intercept laws for accelerating targets. *AIAA J* 1968;**6**(11):2196–8.
13. Cottrell RG. Optimal intercept guidance for short-range tactical missiles. *AIAA J* 1971;**9**(7):1414–5.
14. Turetsky V, Shinar J. Missile guidance laws based on pursuit-evasion game formulations. *Automatica* 2003;**39**(4):607–18.
15. Ge L, Shen Y, Gao Y, Zhao L. Head pursuit variable structure guidance law for three-dimensional space interception. *Chin J Aeronaut* 2008;**21**(3):247–51.
16. Cherry GW. A general, explicit optimal guidance law for rocket-propelled spacecraft. In: *The AIAA/ION astrodynamics guidance and control conference*; 1964 Aug 24-26; Los Angeles, California, USA. Reston: AIAA; 1964. p. 1–2.
17. Ohlmeyer EJ, Phillips CA. Generalized vector explicit guidance. *J Guidance Control Dyn* 2006;**29**(2):261–8.
18. Yu WB, Chen WC. Trajectory shaping guidance with final speed and load factor constraints. *ISA Trans* 2015;**56**:42–52.
19. Wang H, Lin De, Cheng Z. Optimal guidance of extended trajectory shaping. *Chin J Aeronaut* 2014;**27**(5):1259–72.
20. Ben-Asher JZ, Yaesh I. *Advances in missile guidance theory*. Virginia: AIAA Progress in Aeronautics and Astronautics; 1998. p. 25–88.
21. Kim M, Grider KV. Terminal guidance for impact attitude angle constrained flight trajectories. *IEEE Trans Aerosp Electron Syst* 1973;**9**(6):852–9.
22. Ryoo CK, Cho H, Tahk MJ. Time-to-go weighted optimal guidance with impact angle constraints. *IEEE Trans Control Syst Technol* 2006;**14**(3):483–92.
23. Zhao J, Zhou R. Three-dimensional cooperative guidance laws against stationary and maneuvering targets. *Chin J Aeronaut* 2015;**28**(4):1104–20.
24. Yang L, Zhou H, Chen WC. Application of linear gauss pseudospectral method in model predictive control. *Acta Astronaut* 2014;**96**(1):175–87.
25. Hablani HB. Endgame guidance and relative navigation of strategic interceptors with delays. *J Guidance Control Dyn* 2006;**29**(1):82–94.
26. Ratnoo A, Ghose D. Collision-geometry-based pulsed guidance law for exoatmospheric interception. *J Guidance Control Dyn* 2009;**32**(2):669–74.
27. Newman B. Strategic Intercept midcourse guidance using modified zero effort miss steering. *J Guidance Control Dyn* 1996;**19**(1):107–12.
28. Lyzhoft J, Wie B. IR telescope and sensor characterization for hypervelocity asteroid intercept guidance. In: *AAS/AIAA space flight mechanics meeting*; 2014 Jan 26-30; Santa Fe, New Mexico, USA. Reston: AIAA; 2014. p. 1–17.
29. Waldmann J. Line-of-sight rate estimation and linearizing control of an imaging seeker in a tactical missile guided by proportional navigation. *IEEE Trans Control Syst Technol* 2002;**10**(4):556–67.
30. Ben-Asher JZ, Yaesh I. Optimal guidance with reduced sensitivity to time-to-go estimation errors. *J Guidance Control Dyn* 1997;**20**(1):158–63.

Yu Wenbin received the B.S. degree in aerospace engineering from Beihang University in 2010. After that, he was recommended for pursuing the doctor's degree directly also in Beihang University and received it in 2016. Now he is a postdoctoral researcher in Beihang University. His main research interests are flight mechanics, guidance and control.

Chen Wanchun received the B.S., M.S. and Ph.D. degrees in aerospace engineering, Beihang University, Beijing, in 1986, 1989, and 1995, respectively. Since 1989, he has been with the School of Astronautics, Beihang University, where he is currently a Professor and Ph.D. supervisor. His main research interests include flight Mechanics, guidance and control, and trajectory optimization.

Yang Liang received the Ph.D. degree in Beihang University. His research interests are flight mechanics, guidance and control, and trajectory optimization.

Liu Xiaoming is a Ph.D. and lecturer in Beihang University. His research interests are flight Mechanics, guidance and control, information fusion, and sensors applications.

Zhou Hao received his Ph.D degree in Beihang University and then became a lecturer there. His research interests are flight mechanics and trajectory optimization.